SAND2019-11049C

Datasets for Material Ignition from High Radiant Flux

Alexander L. Brown[a*], Jeffrey D. Engerer[b], Allen J. Ricks[c], Joshua Christian[d], Julius Yellowhair[e]

[a]Sandia National Labs, PO Box 5800, Albuquerque, NM, USA, albrown@sandia.gov

[b]Sandia National Labs, PO Box 5800, Albuquerque, NM, USA, jengere@sandia.gov

[c]Sandia National Labs, PO Box 5800, Albuquerque, NM, USA, aricks@sandia.gov

[d]Sandia National Labs, PO Box 5800, Albuquerque, NM, USA, jmchris@sandia.gov

[e]Sandia National Labs, PO Box 5800, Albuquerque, NM, USA, jeyello@sandia.gov

*Corresponding author

Abstract:

High heat flux (>500 kW/m^2) ignitions occur in scenarios involving metal fires, propellants, lightning strikes, above ground nuclear weapon use, etc. Data for material response in such environments is primarily limited to experimental programs in the 1950s and 1960s. We have recently obtained new data in this environment using concentrated solar energy. A portion of the experimental data were taken with the objective that the data be useful for model validation. To maximize the utility of the data for validation of predictive codes, additional focus is placed on repeatability of the data, reduction of uncertainties, and characterization of the environment. We illustrate here a portion of the data and methods used to assess environmental and response parameters. The data we present are novel in the flux range and materials tested, and these data constitute progress in the ability to characterize fires from high flux events.

Keywords: High Radiative Flux; Ignition; validation

1. Introduction

Much of the information in the open literature on ignitions at very high heat flux goes back to the work of Martin et al. in the 1950s and 1960, as well as the above ground nuclear tests of the same era. The work of Martin et al. [1-3] extensively characterized cellulose ignition for a variety of sample thicknesses and flux exposures. Tens of thousands of individual tests contribute to a detailed understanding of the ignition threshold for blackened cellulose materials. Data exist for many more materials, but nothing close to the magnitude of data for cellulose. The work represents a wealth of information provided that ignition of cellulose is representative of the material and response of interest. With the continual improvement of modeling and simulation capabilities as well as experimental techniques, there are new concepts and possibilities that benefit from revisiting the historical work. If a material of interest is outside the ignition regime, it may still be pertinent to know whether the material charred in response to the imposed flux. This information is not available from the Martin et al. work. Also, computational fluid dynamic (CFD) models predict flame luminosity, soot production, velocities, heat transfer, etc. Many of the data necessary to validate these aspects of a prediction are not

Sandia National Laboratories is a multimission laboratory managed and operated by National Technology & Engineering Solutions of Sandia, LLC, a wholly owned subsidiary of Honeywell International Inc., for the U.S. Department of Energy's National Nuclear Security Administration under contract DE-NA0003525.

found in the historical literature [1-4]. Improved model validation is enabled by increasingly detailed high-quality datasets with more comprehensive data on the variety of responses [5].

Over the last several years, several test campaigns have been conducted at the National Solar Thermal Test Facility (NSTTF). A portion of the campaign work has been dedicated to creating data that meets a higher objective of being of increasing worth for validation. For these tests, the number of repeats was increased with respect to the rest of the test series data to better characterize the aleatory uncertainty. The samples tended to be better characterized in terms of shape, size, and source. The materials were selected to be ones that were common such that repetition is facilitated and model characterization of the sample properties has a stronger pedigree. The intent was to build a database of material response at high heat flux to provide the general community with significantly improved information on the behavior of materials at high flux conditions. This will aid in validating computational models like CFD.

An ideal dataset for CFD validation includes comprehensive data for all relevant phenomena predicted by the model. This ideal includes 3D solid temperatures, temporal pyrolytic response of the materials, velocity and species field data, radiation fluxes, etc. Results should include uncertainty estimates and provide details on measurement techniques to permit quantification of error. Simultaneous extraction of all these data is not presently realistic, however, there are techniques that can address most of these in good detail. One of the better examples in the literature of a dataset approaching comprehensive data for pyrolysis in conventional flux conditions was published recently [6]. Others note a current need for improved data in this area [7-8] even for low-flux conditions. While conventional historical data are still insufficient to meet this ideal, the high flux environment is further challenged by the rate at which the phenomena occur and the challenges dealing with high energy environments. High flux CFD validation data are significantly lacking.

This paper details selected results from testing performed at the NSTTF. Selected tests include those that had a higher number of repeat tests (>2) that allow material and experimental variability to be better quantified. This paper focuses less on the comprehensiveness of the report of the data and more on the characterization of the measurement accuracy and reporting of the data in a way that can help validate simulation capabilities. These results have implications as to the test and conditions that may be considered optimal for a detailed validation comparison effort. Additional detailed data may be found in prior publications of the results focusing on other aspects [9-12] as well as in forthcoming test reports.

2. Material and Methods

2.1 Facilities

The National Solar Thermal Test Facility at Sandia National Labs in Albuquerque has two main facilities that concentrate solar energy for general testing. One is the Solar Tower (ST), that uses a heliostat field (an array of large mirrors with fine motor control that actively track the sun to maintain a relatively constant target location for the rays) to achieve a concentration factor greater than 2000 suns (1 sun is approximately 1 kW/m^2), and a power of 6 MW at minimum focal length scales of 0.3-1 m. The other is the smaller Solar Furnace (SF) that uses a single heliostat and a parabolic dish for smaller length scale testing (5-7 cm). Annotated photographs of these are shown in Fig. 1. Several hundred high flux ignition tests have been conducted at these facilities including varying material types, thicknesses and shapes, while also varying flux, fluence, length-scale, wind, and ambient temperature. These tests were performed in four phases, three with the SF and one at the top of the ST. We will identify these with SF or ST followed by the number of the phase of testing throughout the remainder of this document.

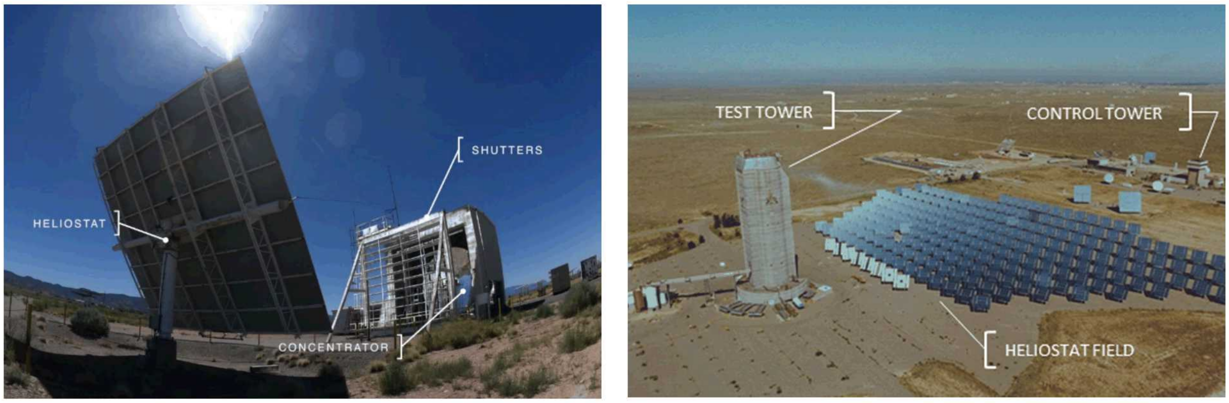

Fig. 1. Annotated photographs of the SF (left) and ST (right) facilities

2.2 Flux Characterization

Flux control and measurement was complex with all the test cases. At the ST, the temporal flux was controlled with a dropping shroud at the front side of the tests and heliostat motors at the tail end. At the SF, a motorized louvered panel dynamically attenuated the solar energy reaching the parabolic dish. The spatial profile for the SF was previously characterized, and a radial fit to the measured distribution is found in [13], with a model for the response as indicated in Fig. 2.

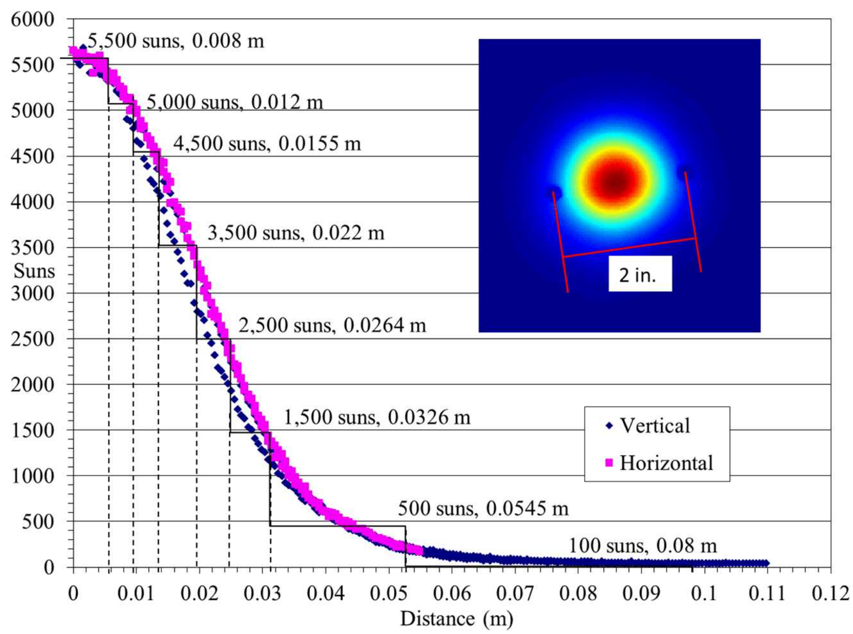

Fig. 2. Experimental flux map from solar furnace, Peak flux is 5700 suns (1 sun = 1 kW/m^2)

At the ST, the spatial profile was evaluated for many of the test scenarios using a ray-tracing algorithm, SolTrace. Examples of a few of these traces are found in Fig. 3. Both facilities used pre- and post-test flux characterization to calibrate the test shots. At the SF, the peak heat flux for each experiment was measured by a radiometer before and after each test. The accuracy of the radiometer yielded 2% epistemic uncertainty. Atmospheric conditions varied during any given testing window, causing uncertainties on what the peak flux was during a given experiment. Random variations recorded across over 100 experiments, revealed approximately normally distributed 1.8% aleatory uncertainty (95% confidence) in peak flux.

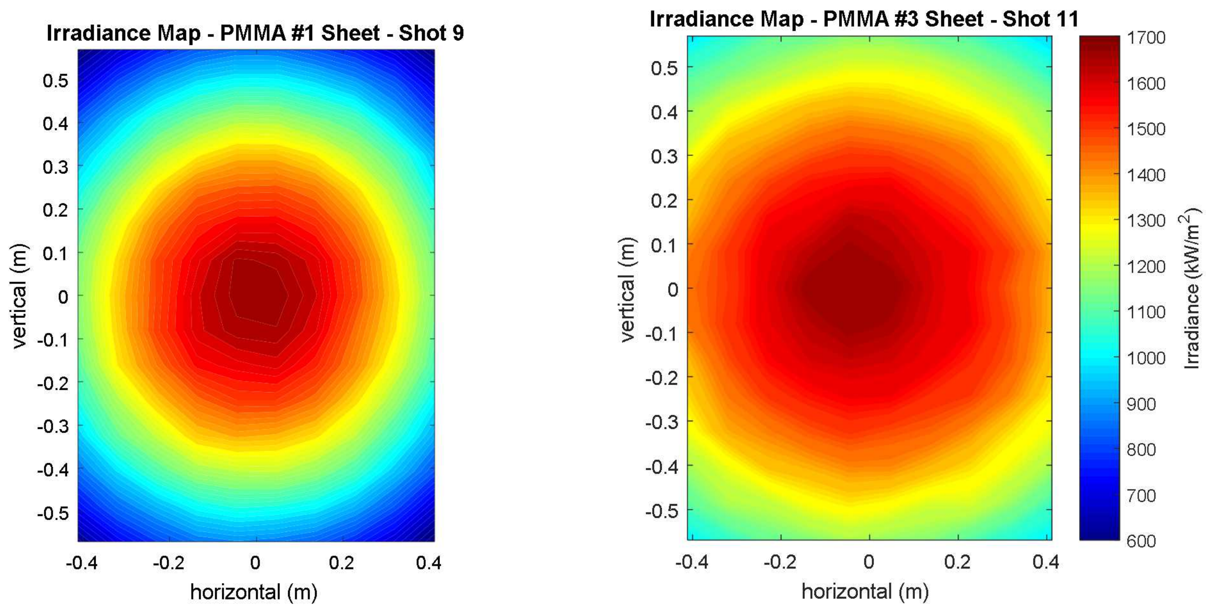

Fig. 3. Example irradiance maps from SolTrace Monte Carlo ray-trace software

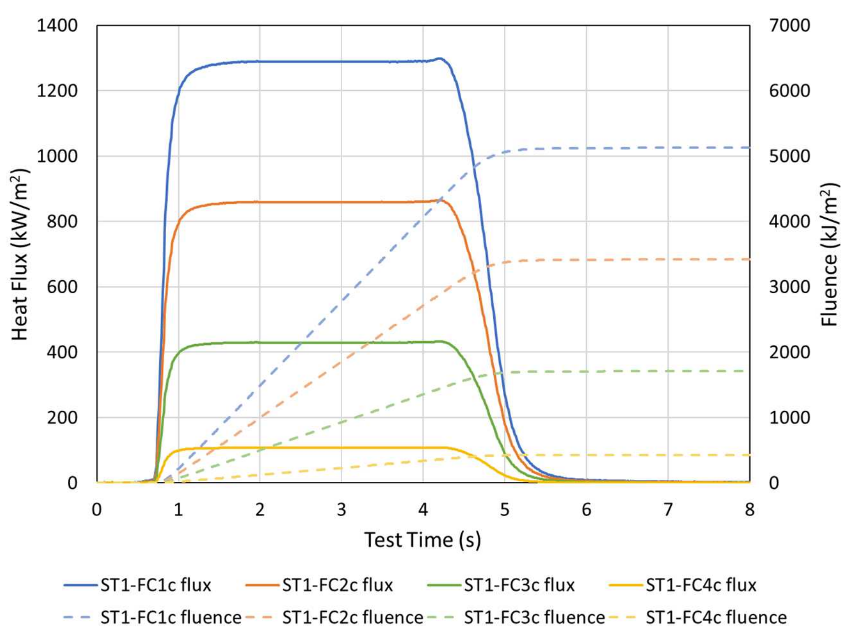

Fig. 4 Example constructed curves used as the basis for ST tests(ST1-FC-c series).

The temporal flux was characterized for both facilities. At the SF, the dynamic heat flux was evaluated using a heat flux gauge before and after each experiment. This process introduced additional aleatory uncertainty, totaling 2.8% (95% confidence) for the dynamic portion of the exposure. The epistemic uncertainty for dynamic heat flux was also 2%. Center fluxes for the SF were characterized for each test. A model for the temporal flux for the ST was used to deduce what was a vertically changing profile as the shutter fell. Characteristic flux curves are illustrated in Fig. 4 and 5 for the ST and SF respectively for example test operations. Models for these temporal responses were generated to aid in interpretation of the results, details of which will be published elsewhere.

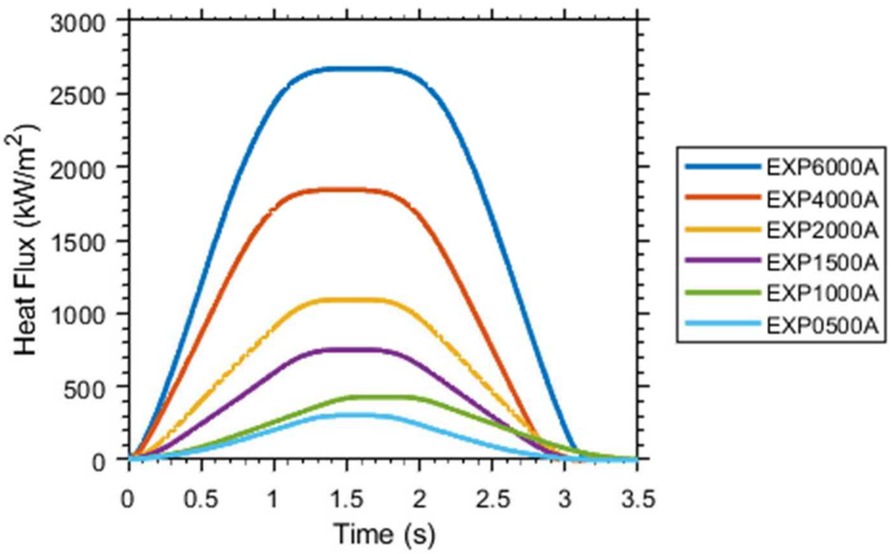

Fig. 5. Example exposure data from the heat flux gauge taken prior to each experiment for SF2.

2.3 Diagnostics

A variety of instrumentation was deployed for the tests, the details of which may be found in the test series documentation. For this paper, highlights of the instrumentation are outlined only. Details on the instrumentation are available in the corresponding test phase documentation and existing literature [9-12]. Each test included the following:

1. Pre- and post-test flux measurements to confirm the imposed thermal environment, and characterization of the day, time, and configuration of the flux source
2. Multiple angle fiducially accurate video imagery from standard, high-speed, and filtered optical cameras
3. Atmospheric data from on-site weather stations to confirm the ambient conditions
4. Pre- and post-test photography
5. A temporal fiducial to allow post-test synchronization of instrumentation results from various sources
6. Controls output containing data on the temporal sequence for each test

Tests mostly included:

1. Pre- and post-test weight of samples

Some tests included:

1. Strategically mounted thermocouples for temperature measurements
2. IR camera imagery for thermal response
3. Witness strings as local air flow indicators
4. Post-test 3D scanning for digital re-construction of the thermal crater

Ignition, mass loss, and burn times are key to the analysis presented in this paper. These were deduced through post-test analysis of the video imagery. Ignition was often discernable through the observed flames in the video output. In some ST tests, the pyrolysis gases obscured direct views of the ignition. The ignition event usually included a rapid increase in the motion of the pyrolysis gases, in which case the flames were not directly observed but inferred based on the motion of the opaque gases and the presence of flaming later in the video. Pyrolysis initiation was potentially confounded by water vapor evaporation. Mindful of this, the analysts used judgement to interpret the pyrolysis initiation time by examining the coloration and form of the cloud and the surface.

2.4 Materials and Test Conditions

While the broader study used a large number and sources of materials, here we are focused on tests with a high number of repeats. These included polymethyl-methacrylate (PMMA; black), high impact polystyrene (HIPS; black and white), cellulose (pressed microcrystalline powder), and black posterboard. Sources for each material are found in Table 1. Most tests exposed flat surfaces with varying thickness.

Table 1 Materials Tested

Sample	Description	Sources	Test
Posterboard	100# Black posterboard, 100% Wood pulp, Linen Pattern, 0.25 mm (0.010") thick	Mohawk Fine Papers, Inc. (seller: Sandia Paper Company, Inc.)	ST1
PMMA	Acrylic sheet, black 2025 opaque, paper, cast poly methyl-methacrylate, 3.175 mm (0.125"), 11.3 mm (0.446") thick	Curbell Plastics Tap Plastic	SF1 ST1 SF2
Polystyrene (HIPS)	High-impact polystyrene sheet, matte/smooth, 3.175 mm (0.125") thick	Curbell Plastics Spartech	SF1 SF2 ST1
Cellulose	Compressed powdered α-cellulose	Aldrich Chemistry 51 μm microcrystalline powder	SF1

One SF campaign (phase 2) occurred during winter, which had significantly lower initial temperatures for materials. Post- test analysis does not suggest a significant dependency of any results to the range of temperatures tested (about 30ºC). Wind on the other hand has a significant effect on the direction of the plume and in some cases on the performance results. Wind was more of a factor for SF1 and the ST1 tests. A wind shield consisting of a three-sided Plexiglas cubic enclosure helped to reduce winds in SF2 and SF3.

3. Results and Discussion

The ability to apply a repeatable condition to the test objects is important. Table 2 shows the repeatability of the imposed conditions for the tests. Table 2 indicates the HIPS color, W for white and B for black. The S for the ST1 PMMA is for small, meaning a small target produced by a common focal point. The L for the ST1 PMMA is for large, meaning the flux condition involved a rectangular arrangement of four aim points that produced a larger target spot and a more uniform peak flux across surfaces. The posterboard and HIPS were tested with a small single aim point flux at the ST.

Table 2. Test results of the repeatability of the environment.

			Flux	*kW/m²*		Fluence	*kJ/m²*	
Material	**Replicates**	**Phase**	μ	σ	**CV (%)**	μ	σ	**CV**
Cellulose	5	SF1	2354.0	47.2	2.0	6046.0	122.2	2.0
PMMA	5	SF1	2386.0	32.9	1.4	6104.0	102.9	1.7
HIPS-W	5	SF1	2426.0	35.8	1.5	6234.0	54.1	0.9
PMMA	3	SF2	1846.7	30.6	1.7	3426.7	60.3	1.8
HIPS-B	4	SF2	1670.0	82.9	5.0	3107.5	142.4	4.6
Posterboard	3	ST1	194.0	1.7	0.9	473.3	5.8	1.2
PMMA-S	3	ST1	1653.3	15.3	0.9	4166.7	40.4	1.0
PMMA-L	3	ST1	1613.3	40.4	2.5	3956.7	90.7	2.3
HIPS-B	4	ST1	1642.5	5.0	0.3	4157.5	9.6	0.2

The largest Coefficient of Variance for heat flux (CV; σ/μ, where μ is the mean and σ is the standard deviation) is for HIPS from the SF2 series, which had a CV of 5.0 %. Good repeatability of the environment is found for these tests. Initial testing for SF1 involved 5 replicates. These were reduced for subsequent test series because the final replicate was deemed to have diminishing value to the results compared to the opportunity to test a broader range of materials at a greater range of conditions.

The standard deviation for initial temperatures was near 1.0 for most tests. Exceptions were the HIPS for SF2, the PMMS-S, and PMMS-L with standard deviations of 8.0, 6.7, and 3.0 respectively. There was not an obvious effect of the initial temperature on the results. Initial temperature means varied from a low of 16.9ºC for the SF2 PMMA up to 36.7 for the HIPS from ST1. Sun exposure augmented initial temperatures, due to radiant heating in some (particularly ST) cases.

3.1 Mass Loss and Winds

One of the main outputs of interest from these tests was the mass loss. Historical work suggests mass loss tends to be linear with fluence beyond the low fluence heat-up regime, which is demonstrated for cellulose [1]. Mass loss was not strictly proportional to the applied fluence. The synthetic polymer materials were prone to lose less mass relative to the energy input at larger scale, a feature not identified in historical work [9]. Table 3 shows mass loss along with ambient wind magnitude and direction data. The ST1 series of tests was more impacted by the wind conditions, a feature whose only practical control was the selection of test days and times.

This is apparent in the generally higher CV for ST1 tests. The cellulose CV was high from the SF1 test. During these tests, the ignition was highly variable, and from analysis of the video appears susceptible to even light smudges and discolorations that were not avoided during handling of the prepared samples. There was also indication of significant ejection of the powder, suggesting the packing of the powder was insufficient to achieve solid-like behavior of the packed bed. Comparable SF2 tests had moderately lower CVs, which is believed to be in part due to the enclosure designed to reduce ambient wind effects. The HIPS in SF1 was white, while it was black in SF2 (as was the cellulose). This may also be a contributing factor.

The wind data are not considered particularly significant for the SF scenarios. The wind was a factor insofar as it disrupted flows. But the SF facility is in a partial enclosure, and for SF2, a partial enclosure inside the facility was constructed. Scenarios with very high wind speeds would be concerning, but these were generally not present. The facility was not operated during high-winds to prevent damage to the heliostats. The wind is a more significant factor for the ST data where there was no partial enclosure. Mass loss appears correlated with wind direction, although the nature of this correlation is not strong due to sparsity of data (indications are not shown here). We conclude that such a relationship exists, but additional data are necessary to better understand it.

Table 3. Mass loss and wind data

		Mass Loss (g)			Wind Speed (m/s)		Wind Direction (º)	
Material	**Phase**	μ	σ	**CV (%)**	μ	σ	μ	σ
Cellulose	SF1	2.20	0.56	25.51	2.92	1.54	241.40	39.39
PMMA	SF1	5.66	0.28	4.93	3.00	1.12	229.20	75.51
HIPS-W	SF1	0.54	0.05	10.14	3.14	0.75	237.40	98.07
PMMA	SF2	2.60	0.09	3.33	4.10	2.25	281.67	11.06
HIPS-B	SF2	0.85	0.07	7.74	5.10	0.80	209.75	40.38
Posterboard	ST1	32.67	7.02	21.50	1.50	0.10	205.00	49.57
PMMA-S	ST1	260.00	97.00	37.31	3.00	1.95	188.67	22.50
PMMA-L	ST1	959.00	847.11	88.33	3.10	0.50	262.00	81.66
HIPS-B	ST1	165.00	29.70	18.00	2.80	0.93	264.00	73.96

3.2 Ignition

A key analysis point from this work is the ignition time. It relates through knowledge of the flux profiles to the ignition threshold. This is a focus of historical studies. In addition to the focus on ignition thresholds, we also focus on the first indications of pyrolysis occurring. This is potentially confounded with moisture evaporation from hygroscopic materials. Identification of ignition can be challenging, especially in the ST experiments with a larger and more opaque plume formed on initiation of pyrolysis. Table 4 provides data for the ignition and pyrolysis initiation times and the initial and ambient temperatures. Lack of reported ignition times suggests samples did not ignite. Lack of pyrolysis initiation times reflects lack of identification of the times (for PMMA SF1, the initiation times are not reported).

Table 4. Ignition and pyrolysis temporal initiation times [s] and temperature [ºC] data

		Pyrolysis (s)			Ignition (s)			Initial T	Ambient T
Material	**Phase**	μ	σ	**CV (%)**	μ	σ	**CV (%)**	μ	μ
Cellulose	SF1	1.10	0.34	30.83	1.24	0.27	21.70	32.54	29.66
PMMA	SF1							39.80	30.42
HIPS-W	SF1	1.10	0.16	14.37	1.38	0.11	7.66	33.30	29.60
PMMA	SF2	0.77	0.04	4.68				16.87	7.03
HIPS-B	SF2	0.33	0.03	10.09	0.86	0.05	6.20	30.60	17.18
Posterboard	ST1	1.23	0.01	0.94					16.00
PMMA-S	ST1	0.67	0.05	7.90	1.12	0.20	17.43	29.20	20.47
PMMA-L	ST1	0.65	0.04	6.19	1.03	0.01	0.56	28.43	14.73
HIPS-B	ST1	0.66	0.05	8.30	0.84	0.11	12.99	36.68	13.80

The repeatability of the ignition times is mixed, with the cellulose SF1 test, the PMMA-S ST1, and the HIPS ST1 tests with the largest CVs. Some of the surface related issues (discoloration and particle ejection) with the Cellulose SF1 tests have already been mentioned and are believed to be a factor here. The ST1 ignition times are not as easy to identify due to plume blocking effects, contributing to the epistemic uncertainty with these data. Accuracy for some of the shots is within a few frames instead of a single frame as with the SF data and some of the ST data. It is not clear how much wind magnitude and direction play a role in the spread of ignition time data. The pyrolysis initiation times mostly exhibited much lower CV for the datasets that had high ignition CV. The pyrolysis initiation times were least repeatable for the white materials (cellulose and HIPS from SF1). The ST1 Posterboard tests had the lowest CV, and the rest were all about 5.0% and greater. Repeatability is challenged by the temporal accuracy because of the short time frames over which the exposure initiation to pyrolysis and ignition occur.

The average temperature of both the sample and the ambient conditions is also given in Table 4. The samples were warmer than the ambient temperature at the start of tests by around 10.6 ºC on average. Ambient temperatures were taken higher in the atmosphere, so samples were likely influenced by solar heating of the ground near noon in the surface boundary as well as by solar radiation for exposed samples. ST1 samples generally had the highest differences between ambient and initial temperatures.

The posterboard samples did not ignite, which limits the utility of the data. The flux/fluence condition for this test was near the ignition threshold for the samples as suggested by the work of Martin et al., and because some initial testing suggested a higher propensity for ignition at larger-scale, this condition was thought to be a good test target that would not over-expose the material. After the first few tests did not achieve ignition, the decision was made to continue with the tests at present conditions to achieve the goal of having a high replicate test set for a mostly cellulosic material. PMMA did not ignite for SF1 and SF2, but readily ignited in ST1 with lower fluxes. This represents a significant scale effect, the subject of a paper previously written [9].

3.3 Imagery

Photometric imagery plays an important role in deducing several response parameters of interest. Ignition and pyrolysis initiation times have already been described. The pyrolysis and flaming regions often are identifiable by relatively sharp image thresholds in the test imagery and constitute a contribution to the description of the test results that can be used to infer velocities and plume dynamics. We have employed edge detection methods to extract plume shapes, and also looked at particle tracing algorithms to deduce velocities [14]. Post-test images coupled with the temporal/spatial characterization give information on minimum requirements to initiate charring.

Here we elect to simply illustrate tiled images from the tests to show the general time evolution of the plumes for selected tests. A more comprehensive set of these images is available in the test documentation. Fig. 6 shows filtered imagery for the SF1 tests. Two synchronized views are present for each time and material. The filtering made it difficult in many cases to identify with confidence the ignition time due to lack of color and resolution of the flames over the incident flux, resulting in the addition of cameras for subsequent test phases.

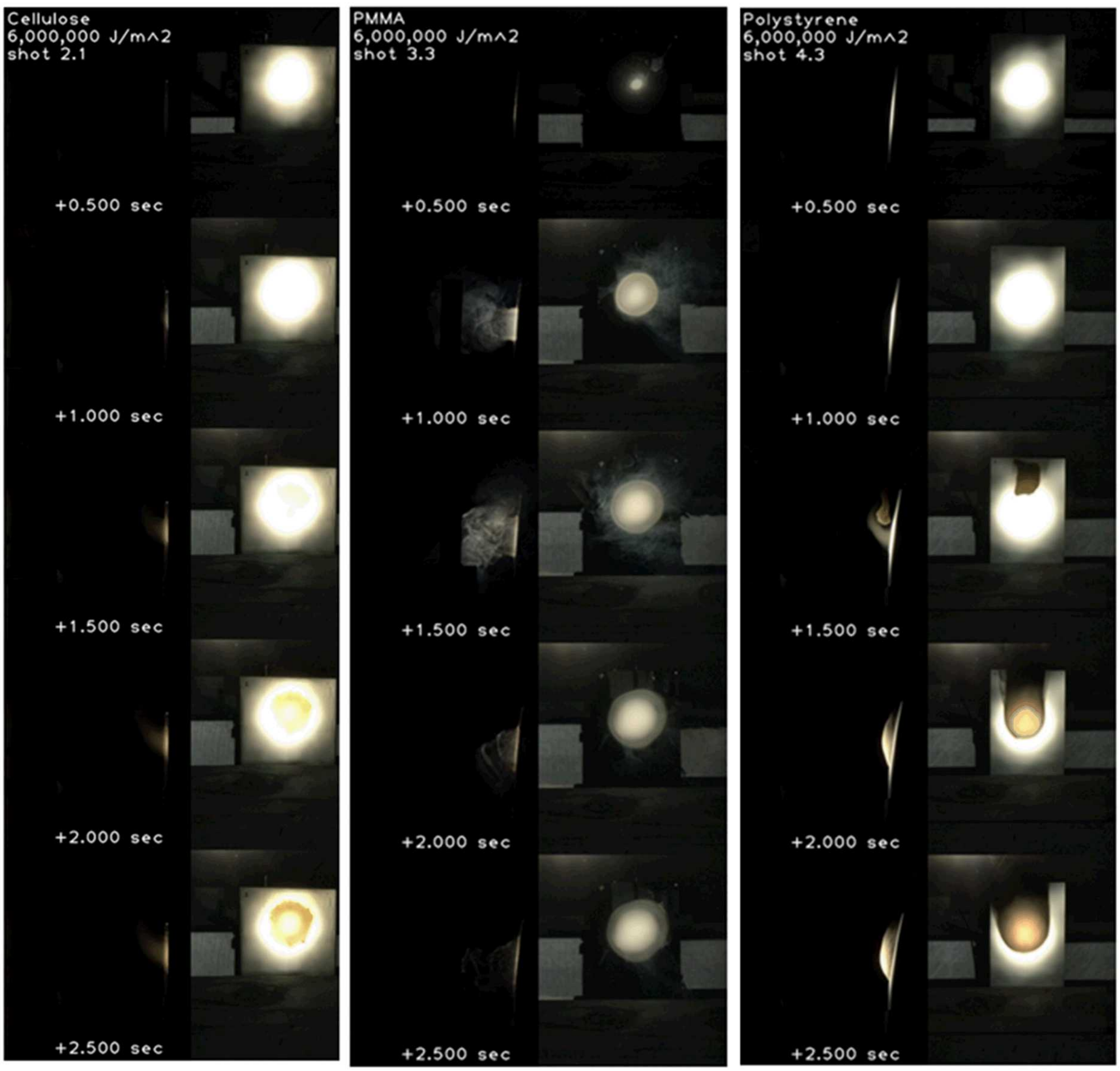

Fig. 6. Tiled frames from SF1 tests (synchronized side and front views), cellulose (left) test 1, PMMA (center) test 3, and HIPS (right) test 3.

Fig. 7 shows selected tiled images from SF2 tests. Some fonts may be too small to read in these images, but the white scale lines represent 8 cm length scales and the rest of the information is redundant. Flaming is more apparent in the unfiltered frames on the left, while the right images that are filtered avoid saturation to better observe the material response.

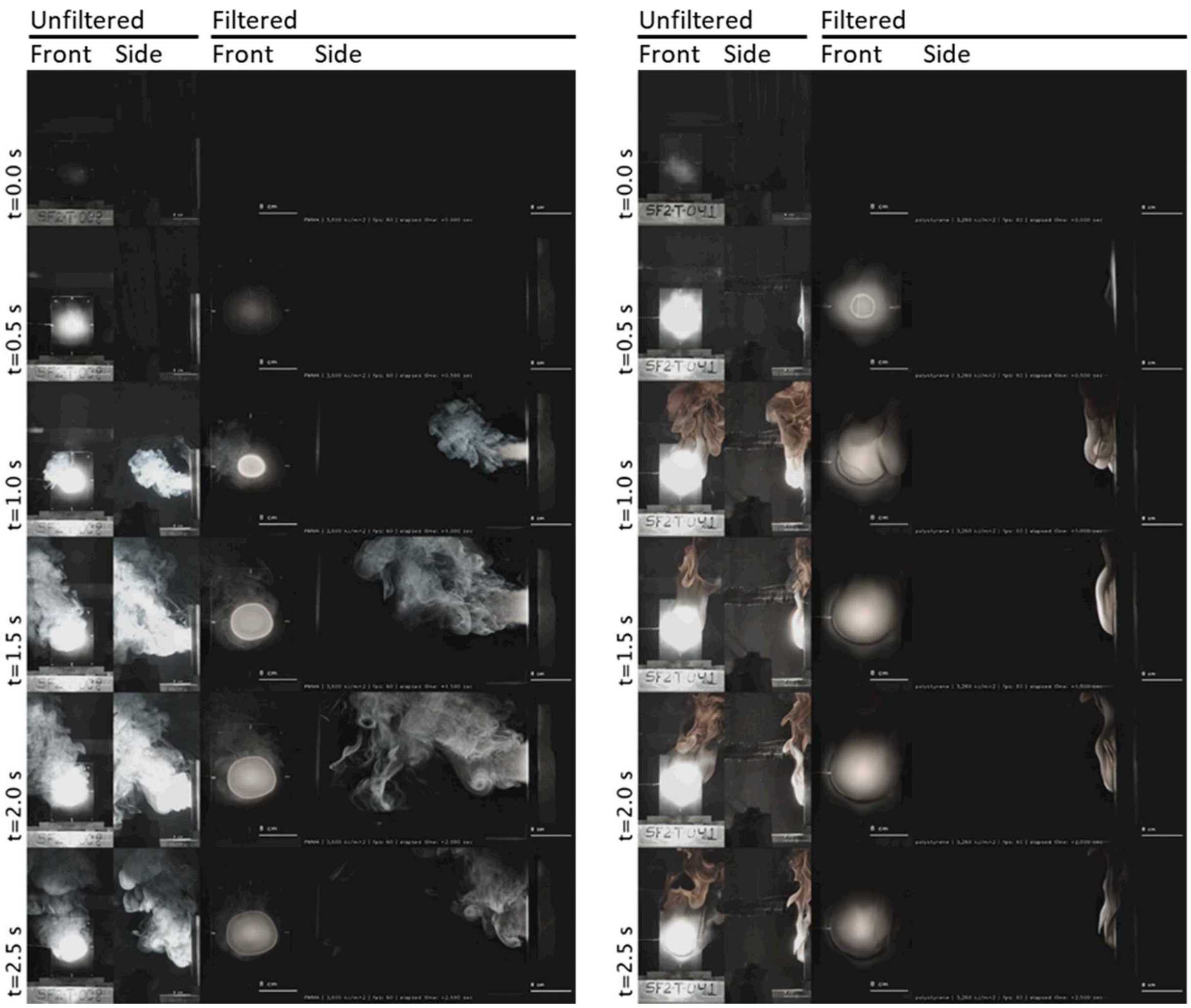

Fig. 7. Synchronized tiled frames from four cameras for SF2 PMMA (left) sample 1, and HIPS (right) sample 1.

Images from selected ST1 tests from the side with similar general wind directions are found in Fig. 8. Some tests were performed with opposite winds, but were lower in frequency. The first frame at t=0.0 s shows the shroud in place that blocked radiation until the desired start time. It rapidly dropped (<1 second), exposing the sample. Subsequent frames show dynamics of the plume due to material response. For scale reference, the samples were 1.22 m high

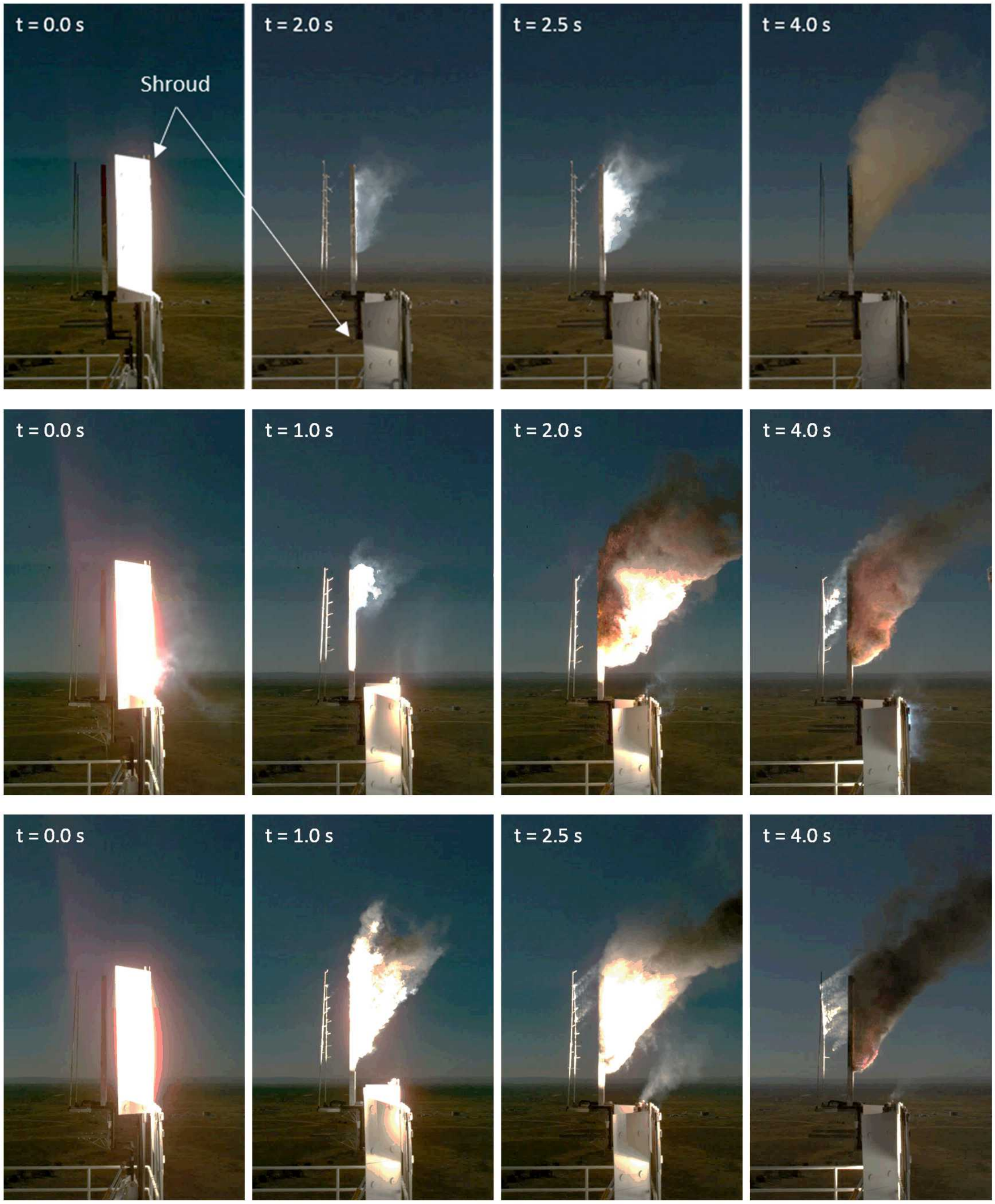

Fig. 8. Stills from the side for ST1 posterboard (top) test 4, PMMA (middle) test 2, and HIPS (bottom) test 4. The heliostat field is to the right.

Although selected images are shown here, there was a range of image response. Lacking a good way to capture that in this paper, we show representative images. A validation study requiring variability in response will benefit from accessing the full range of response of all output figures that would not fit this paper, but can be accessed in other documentation.

3.4 3D Scans

Many SF test samples were scanned after testing to produce digital representations of the cavity formed by the flux exposure [15,16]. ST samples were cut and post-test thickness was measured with a micrometer at selected locations. The SF1 series had difficulties with post-test scanning of the samples. The cellulose appears to have swollen in its metal holder, possibly due to gases pressurizing and causing internal swelling. The PMMA and HIPS samples distorted significantly due to the exposure in SF1, complicating the post-test analysis of the shapes. The white samples were also more diathermal than the dark samples, which is a complication that is undesirable for datasets when other complicating factors are still not particularly well understood. For SF2, the PMMA samples were much thicker and resisted distortion. These data are the best of the scanned data, and example output is shown in Fig. 9. The HIPS in SF2 and ST1 did not exhibit as significant change in thickness. This is postulated to be due to swelling of the sample or char formation, as mass was clearly lost in these tests. The posterboard for ST1 was brittle post-test, and unreliable to analyze for thickness post-test. The PMMA ST1 samples exhibited significant thinning, with a plot of the spatial variation of mass loss indicating increased mass loss (decreased thickness) lower on the sample, as shown in Fig. 10. There was almost a millimeter variation in thickness, and the resulting change in thickness was not as radially uniform as was the case for the SF test results. Scale reference for this figure is the panel was 914 mm wide by 1219 mm high, with the center point in the middle of the panel and horizontal spacing of 229 mm and vertical spacing of 205 mm.

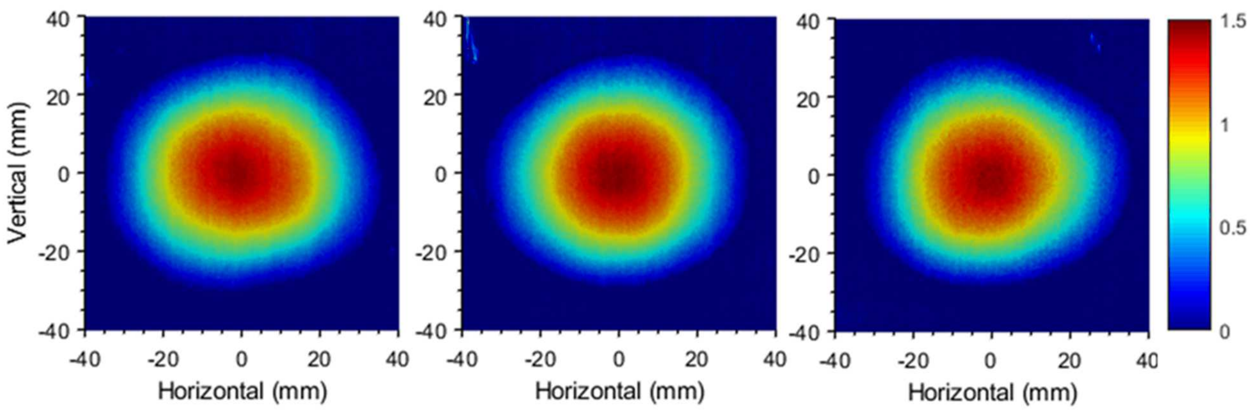

Fig. 9. Crater depths for SF2 PMMA Sample 1 (left), Sample 2 (middle), and Sample 3 (right) obtained via 3D Scanner.

3.5 General Discussion

The data presented here represent some well characterized exposure conditions for materials in response to high heat flux conditions. While not all data were successfully repeatable to a standard of low CV, there are sufficient data that fell below CV of 5% that there are good prospects for validating a simulation tool with these data. Repeatability was challenged by several sources of error. Some of the materials were not prepared in a way that they resulted in high repeatability (e.g. SF1 cellulose), while the wind was a factor in some of the experiments (SF1 velocity fields and ST1 mass loss). Efforts were made to reduce variability in the solar irradiance, and the good repeatability of the flux conditions suggests the efforts were largely successful. The datasets that lack repeatability might be helpful to repeat or improve in the future to increase the range and quality of validation data in this thermal regime.

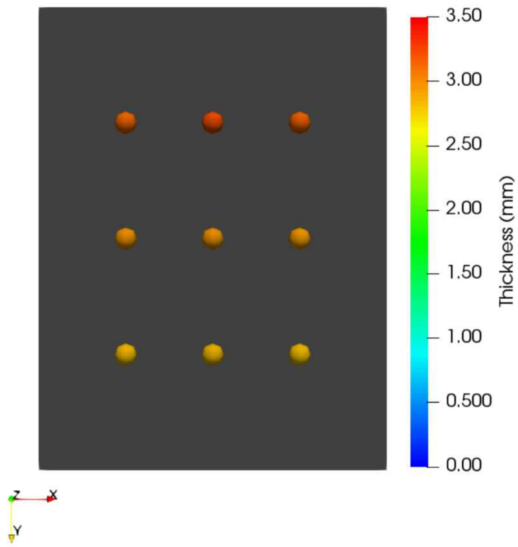

Fig. 10. Post-test thickness of PMMA small-spot Sample 2 looking from the north.

We have omitted several existing data aspects of the broader test results in this paper, including temperature measurements from some samples, infrared camera results from selected tests, detail time related imagery data, and pre- and post-test imagery. Additional significant video data exist, especially at the ST where results are shown here for only one view angle. These might also contribute to a validation study, providing a high level of detail for characterizing model versus experiment accuracies, and should be examined if a detailed validation study is part of follow-on work. The results selected for presentation here were intended to give an overview of the data with uncertainties and enough information for a cursory validation effort.

Much of the data from the test series were not exhibited in this report. Because we used a minimum number of 3 replicates as a selection criterion, we omitted a large amount of potentially relevant data. If the replicate requirement on the data is relaxed to 2, there are a large number of additional data that might be useful. One might argue that the ST tests did not achieve the repeatability requirements as the wind was actually a discriminating factor. This is probably a valid argument for the mass loss and plume data, but we don't believe pyrolysis initiation is similarly sensitive. Near total lack of similarly scaled data in historical work at high flux conditions is also motivation to retain these data in the published results. For generalized ignition modeling, a breadth of materials and conditions are desirable, and there remains significant potential for additional work in this area at this scale to have a complete understanding of how ignitions occur at very high heat fluxes for all material types and shapes.

None of the data were in a regime where the outcome in terms of ignition or non-ignition was variable from test-to-test. This is suggestive of good repeatability, and also helpful for validation because it provides confidence in the resultant behavior. There is value in having data near the ignition threshold, and many of the tests were not particularly close to this limit. This might be a topic for future data selection. Another topic of future work might be to reduce the uncertainties from the larger-scale tests. The wind was a factor that had no practical control for ST tests, and this was found to be a greater factor than anticipated. Lacking control, an increased number of test replicates would eventually produce a range of wind condition responses that could be parsed for a validation quality condition. This would be very valuable to have, as one of the clear outcomes of the test program was a new appreciation for the substantial differences possible in material response from similar flux/fluence conditions but at different scales [9].

4. Conclusions

Good repeatability is mostly attained in the high heat flux (>500 kW/m^2) ignition and response testing performed on several materials. The repeatability provides uncertainty bounds that can be used for assessing the quantitative predictive accuracies of CFD and other such predictive models for high flux ignitions. The breadth of data includes several flux conditions, three material types (cellulosic, PMMA and HIPS), and a variety of instrumentation outputs including mass loss, ignition and pyrolysis initiation times, post-test scans, and imagery. These are novel data that represent a significant expansion to the body of work on material ignition at high heat fluxes.

5. Acknowledgements

The photometrics team at Sandia including Scott Walkington, Mike Montoya, Anthony Tanbakuchi, and Alvaro Cruz-Cabrera provided diagnostic support. The solar tower team including Benson Tso, Roger Buck, Rip Winkel, and Daniel Ray were also key to the operational success. Jon Rogers provided programmatic support for the effort. Student test support from Bobby Thomas, Noah Siegel, and Jeff LaRocco was key. Manuscript reviews by Randy Shurtz and Walt Gill are appreciated. Sandia National Laboratories is a multimission laboratory managed and operated by National Technology and Engineering Solutions of Sandia, LLC., a wholly owned subsidiary of Honeywell International, Inc., for the U.S. Department of Energy's National Nuclear Security Administration under contract DE-NA-0003525.

6. References

[1] Martin, S., 1965, January. Diffusion-controlled ignition of cellulosic materials by intense radiant energy. In Symposium (International) on Combustion Vol. 10, No. 1, pp. 877-896.

[2] Martin S. B. "Fire setting by nuclear explosion: A revisit and use in nonnuclear applications," Journal of Fire Protection Engineering Vol. 14 No. 4, 2004, pp. 283-97.

[3] Butler, C.P., Martin, S.B. and Lai, W., 1956. Thermal Radiation Damage to Cellulosic Materials. Part II. Ignition of Alpha Cellulose by Square-wave Exposure (No. USNRDL-TR-135; AFSWP-906; Project NS 081-001). Naval Radiological Defense Lab., San Francisco.

[4] Glasstone, S. and Dolan, P.J., 1977. The effects of nuclear weapons. DEPARTMENT OF DEFENSE WASHINGTON DC.

[5] Oberkampf, W.L. and Roy, C.J., 2010. Verification and validation in scientific computing. Cambridge University Press.

[6] Pizzo, Y., Lallemand, C., Kacem, A., Kaiss, A., Gerardin, J., Acem, Z., Boulet, P., and Porterie, B., "Steady and transient pyrolysis of thick clear PMMA slabs," Combustion and Flame, 162, 226-236, 2015.

[7] Wong, W. C.-K., Dembsey, N.A., Alston, J., and Lautenberger, C., "A multi-component dataset framework for validation of CFD flame spread models," Journal of Fire Protection Engineering, 23:2, pp. 85-134, 2013.

[8] Gómez, M.A., Porteiro, J., Patiño, D. and Míguez, J.L., 2014. CFD modelling of thermal conversion and packed bed compaction in biomass combustion. Fuel, 117, pp.716-732.

[9] Brown, A.L., Engerer, J.D., Ricks, A.J., and Christian, J.M., "Scale Dependence of Material Response at Extreme Incident Radiative Heat Flux," The 2018 ASME/AIAA Joint Thermophysics and Heat Transfer Conference, Atlanta, Georgia, June 25-29, 2018. SAND2018-5209C.

[10] Brown, A.L., Engerer, J.D., Ricks, A.J., and Christian, J.M., (2019) "Ignition from High Heat Flux for Flat Versus Complex Geometry", 9th Symposium on Fire and Explosions Hazards, April 21-26, St. Petersburg, Russia, pp. 970-979. (SAND2018-10277C).

[11] Ricks, A.J., Brown, A.L., and Christian, J.M. "Flash Ignition Tests at the National Solar Thermal Test Facility," The 2018 ASME/AIAA Joint Thermophysics and Heat Transfer Conference, Atlanta, Georgia, June 25-29, 2018. SAND2018-5414C.

[12] Engerer, J.D., Brown, A.L., and Christian, J.M. "Ignition and Damage Thresholds of Materials at Extreme Incident Radiative Heat Flux," The 2018 ASME/AIAA Joint Thermophysics and Heat Transfer Conference, Atlanta, Georgia, June 25-29, 2018. SAND2018-5257C.

[13] Ho, C.K., Khalsa, S.S. and Siegel, N.P., 2010, January. Analytical methods to evaluate flux distributions from point-focus collectors for solar furnace and dish engine applications. In ASME 2010 4th International Conference on Energy Sustainability (pp. 501-509). American Society of Mechanical Engineers.

[14] Brown, A.L., Anderson, R.R., Tanbakuchi, A., and Coombs, D., "Diagnostics and Testing to Assess the Behavior of Organic Materials at High Heat Flux," 4th Thermal and Fluids Engineering Conference (TFEC) April 14–17, 2019 Las Vegas, NV, USA, TFEC-2019-27457.

[15] Engerer, J.D., Brown, A.L., "Spatially Resolved Analysis of Material Response to Destructive Environments Utilizing Three-Dimensional Scans," The 2018 ASME/AIAA Joint Thermophysics and Heat Transfer Conference, Atlanta, Georgia, June 25-29, 2018.

[16] Engerer, J.D., Brown, A.L., "Pyrolysis under Extreme Heat Flux Characterized by Mass Loss and Three-Dimensional Scans," 4th Thermal and Fluids Engineering Conference (TFEC) April 14–17, 2019 Las Vegas, NV, USA.